

Designing Heisenberg-limited linear detectors—a bottom-up approach

Joe Bentley,¹ Hendra Nurdin,² Yanbei Chen,³ Xiang Li,³ and Haixing Miao¹

¹*Institute for Gravitational Wave Astronomy, School of Physics and Astronomy,
University of Birmingham, Birmingham B15 2TT, United Kingdom**

²*School of Electrical Engineering and Telecommunications,
University of New South Wales, Sydney 2052, Australia*

³*Theoretical Astrophysics 350-17, California Institute of Technology, Pasadena, California 91125, USA*

(Dated: March 21, 2022)

We develop a systematic approach to realising linear detectors that saturate the Heisenberg limit. First, we consider the general constraints on the input-output transfer matrix of a linear detector. We then derive the physical realization of the most general transfer matrix using the quantum network synthesis technique, which allows for the inference of the physical setup directly from the input-output transfer matrix. By exploring the minimal realization which has the minimum number of internal modes, we show that such detectors that saturate the Heisenberg limit are internal squeezing schemes. Then, investigating the non-minimal realization, which is motivated by the parity-time symmetric systems, we arrive at the general quantum non-demolition measurement.

I. INTRODUCTION

The sensitivity of high-precision optical measurements is constrained by the quantum Cramer-Rao Bound (QCRB) which states that the variance of the measured signal due to noise is inversely proportional the variance σ_{NN} of the photon number of the probe degree of freedom coupled to the signal [1–6]. This quantity is ultimately limited by the Heisenberg limit $\sigma_{NN} = N^2$, which states that the uncertainty scales quadratically with the number of resources available (in this case photons), although for most resonant detectors it is often constrained by the stronger shot noise limit (also called the standard quantum limit in quantum metrology): $\sigma_{NN} = N$ [7]. This shot noise limit can be surpassed using techniques such as external squeezing [8] and bandwidth broadening via negative dispersion [9–12], however using these techniques the Heisenberg limit is not saturated. Previously the Heisenberg limit for phase measurement has been saturated in a non-resonant detector using a combination of entanglement, multiple sampling, and probabilistic adaptive measurements [13]. Theoretical examples of systems that saturate the limit have also been derived for exotic non-classical states [14, 15] and using quantum error correction [16]. Here we instead focus on linear optical phase measurement and an alternative approach to saturating the Heisenberg limit. In this paper we introduce a general approach to realising a Heisenberg limited detector directly from its input-output transfer matrix. This approach leads to both minimal and non-minimal realizations: the minimal realization of the general transfer matrix exhibits internal squeezing, directly increasing the photon number fluctuation in the probe degree of freedom, as explored in [17–19]; the non-minimal realization begins with the minimal realization of a first-order lossless passive detector that

does not saturate the Heisenberg limit, then adds a pair of auxiliary modes that result in an infinite signal amplification at DC (i.e. for low frequency signals). The later is motivated by the parity-time (PT) symmetric system explored in [20, 21]. In both cases, we use the systematic realisation framework developed in [22] to realise the simplest single degree-of-freedom system with squeezing, which can be extended to arbitrarily many degrees-of-freedom using this framework. For the signal amplification case, the input-output relation must remain the same so that additional noise channels are not added, and we derive the corresponding conditions for modifying a system’s internal dynamics without affecting its input-output transfer matrix. Additionally we show that this is related to an ideal QND (quantum non-demolition) measurement [23, 24], and quantum-mechanics-free subsystems [25]. Further we show how the dynamics can be arbitrarily modified by adding additional hidden modes while maintaining the QND property of the variable, for example so that the detector’s most sensitive frequency can be tuned to a specific frequency, not limited to DC. In all cases we start with the system’s transfer matrix, since the order of a system’s input-output transfer matrix determines the complexity of the minimal realisation of the system, specifically determining the number of internal degrees of freedom of the system [26]. In this way we can then start with full control on the complexity of the resulting detector in the design process.

The outline of this paper is as follows. In Section. II we define the transfer matrix used to analyse the linear systems in this paper. In Section. III we will show how quantum network synthesis can be used to find a physical realisation directly from the transfer matrix, and how the resulting detector’s performance can be evaluated using the Quantum Cramér-Rao bound. In Section. IV we will then discuss the various conditions on the transfer matrix arising from the physical realizability conditions, which specifies the number of parameters needed to describe a physically realisable system. In Section. V we consider the minimal realisation of the first-order trans-

* Corresponding author: joe.bentley@uni-hamburg.de

fer matrix that saturates the Heisenberg limit, showing that it is an internal squeezing scheme. In Section. VI we consider the non-minimal realisation that saturates the Heisenberg limit by augmenting a tuned cavity with auxiliary modes that do not affect the input-output dynamics, leading to a saturated signal amplification, and further that an ideal QND measurement is realized. It must be stressed that in both cases the infinite signal response is a mathematical artifact of our analysis, which breaks down as the uncertainty becomes comparable to the mean, and therefore we are fundamentally Heisenberg-limited.

II. THE TRANSFER FUNCTION OF LINEAR SYSTEMS

In this work we are concerned with quantum systems with linear dynamics in the Heisenberg picture [27]. In this section we briefly review some of the relevant concepts with further details deferred to Appendix A. Their dynamics are given in the general form

$$\begin{aligned}\dot{\mathbf{x}} &= \mathbf{A}\mathbf{x} + \mathbf{B}\mathbf{u} \\ \mathbf{y} &= \mathbf{C}\mathbf{x} + \mathbf{D}\mathbf{u},\end{aligned}\quad (1)$$

where \mathbf{x} are the operators for the internal modes, \mathbf{u} are the input operators to the system, and \mathbf{y} are the output operators from the system, and they are in general column vectors with operator entries; \mathbf{A} , \mathbf{B} , \mathbf{C} , and \mathbf{D} are complex matrices of the appropriate dimensions compatible with \mathbf{u} , \mathbf{x} and \mathbf{y} . In particular, \mathbf{A} is a square matrix. In this paper we will restrict the analysis to single-input single-output (SISO) quantum systems with the input and output fields each described by a pair of bosonic annihilation and creation operators or quadratures in the two-photon formalism described by Caves and Schumaker [28, 29]. The output \mathbf{y} has the decomposition $\mathbf{y} = \mathbf{y}_n + \mathbf{y}_f$, where \mathbf{y}_n and \mathbf{y}_f are the natural response and forced response, respectively, given by:

$$\begin{aligned}\mathbf{y}_n(t) &= \mathbf{C}e^{At}\mathbf{x}(0-), \\ \mathbf{y}_f(t) &= \int_{0-}^t \mathbf{C}e^{A(t-\tau)}\mathbf{B}\mathbf{u}(\tau)d\tau + \mathbf{D}\mathbf{u}(t),\end{aligned}$$

where $\mathbf{x}(0-)$ is the initial condition for \mathbf{x} at time $t = 0^-$ just before $t = 0$. The natural response only depends on the initial condition $\mathbf{x}(0-)$ but not the input \mathbf{u} while the forced response is the system's output response to the input \mathbf{u} and does not depend on $\mathbf{x}(0-)$.

For causal systems, the impulse response or Green's function h for the system is given by $h(t) = \mathbf{C}e^{At}\mathbf{B}\Theta(t) + \mathbf{D}\delta(t)$ where $\Theta(t)$ is the Heaviside step function. Note that \mathbf{y}_f is the convolution of h with \mathbf{u} . If $h(t) = O(e^{\sigma t})$ then system's transfer function is a complex function defined by:

$$H(\Omega) = \int_{0-}^{\infty} h(t)e^{i\Omega t}dt, \quad \Im\{\Omega\} > \sigma. \quad (2)$$

To conclude this section, we note that the transfer function coincides with the unilateral (one-sided) Laplace transform $\mathcal{L}[h](s) = \int_{0-}^{\infty} h(t)e^{st}dt$ of h with the identification $s = i\Omega$ (note that in many fields, for example the quantum control community as in [26], the Laplace transform is defined with s replaced by $-s$).

III. QUANTUM CRAMÉR-RAO BOUND

In this section we show how the Heisenberg limit can be saturated by minimising the Quantum Cramér-Rao Bound (QCRB) [30]. This is performed by engineering diverging transfer functions from the vacuum input to the probe degree-of-freedom. As stressed previously, any divergent response we engineer is a mathematical artifact and the system will actually be limited by the fundamental Heisenberg limit.

The QCRB sets a lower limit on the variance of an unbiased estimator of a classical signal $x_c(t)$ coupled to a detector linearly via $\hat{H}_{\text{int}} = -\hat{F}x_c(t)$,

$$S_{xx}(\Omega) > \frac{\hbar^2}{S_{FF}(\Omega)} \equiv \sigma_{xx}^{\text{QCRB}}(\Omega), \quad (3)$$

where $S_{xx}(\Omega)$ is the single-sided displacement spectral density and $S_{FF}(\Omega)$ is the power spectral density describing the quantum fluctuations of \hat{F} that couples to the classical signal. In this paper we consider lossless systems, and so the spectral density of \hat{F} is given by,

$$S_{FF}(\Omega) = S_{uu}(\Omega)|G_{uF}(\Omega)|^2 = |G_{uF}(\Omega)|^2, \quad (4)$$

where $G_{uF}(\Omega)$ is the open-loop transfer function from the input \hat{u} to the internal degree-of-freedom \hat{F} which belongs to the vector of internal modes \mathbf{x} . With external squeezing we decrease the QCRB by increasing $S_{uu}(\Omega)$ which is a well known technique, so here we have restricted the input to a unsqueezed vacuum input: $S_{uu}(\Omega) = 1$.

For simplicity we illustrate the general process using an optical interferometer with a Fabry-Pérot cavity, where the probe fluctuation is related to the intracavity photon number fluctuation by,

$$S_{FF}(\Omega) = |G_{uF}(\Omega)|^2 = \frac{\hbar^2\omega_0^2}{L^2}S_{NN}(\Omega), \quad (5)$$

where $S_{NN}(\Omega)$ is the power spectral density of the photon number fluctuations, ω_0 is the laser carrier frequency, and L is the arm cavity length. In this case we measure the displacement $x_c(t)$ and therefore a good figure of merit is the signal-to-noise ratio,

$$\text{SNR} = \int_0^{\infty} \frac{d\Omega}{2\pi} \frac{|x_c(\Omega)|^2}{S_{xx}(\Omega)}. \quad (6)$$

For a displacement spectrum that is flat (frequency independent): $|x_c(\Omega)| = |x_c|$, this SNR is bound by the

QCRB,

$$\text{SNR} \leq \int_0^\infty \frac{d\Omega}{2\pi} \frac{|x_c|^2}{\sigma_{xx}^{\text{QCRB}}(\Omega)} = \frac{|x_c|^2}{\hbar^2} \int_0^\infty \frac{d\Omega}{2\pi} |G_{uF}(\Omega)|^2 = \frac{\omega_0^2 |x_c|^2}{L^2} \sigma_{NN}, \quad (7)$$

and σ_{NN} is total variance of the photon number of the probe degree of freedom. Therefore by maximizing $|G_{uF}(\Omega)|^2$, we maximize the probe fluctuation $S_{FF}(\Omega)$ and the photon number variance σ_{NN} , therefore minimizing the QCRB and maximizing the SNR.

The general approach for realising an optimal detector is then performed as follows. First, as shown in [22], we can synthesise any n degree-of-freedom system directly from its input-output transfer matrix, so long as it obeys certain conditions which will be discussed in Section. IV. Then, labelling each internal degree-of-freedom of the realisation as \hat{F}_i , $i = 1, \dots, n$ we can then calculate the open-loop transfer functions from the input to those degrees of freedom, $G_{uF_i}(\Omega)$. Finally, we can then maximise the right-hand-side of Eq. (7) by maximising $G_{uF_i}(\Omega)$ for the optimal system parameters and also choosing the optimal internal degree-of-freedom \hat{F}_i to couple the signal $x(t)$ to, giving us a systematic way of optimising the detector design given the input-output transfer matrix.

IV. GENERAL CONSTRAINTS ON THE INPUT-OUTPUT RELATIONS OF LINEAR DETECTORS

When considering the most general transfer matrix to realise, we can eliminate a large number of possibilities by considering whether the given transfer matrix is physically realisable, i.e. whether or not it can lead to dynamics that preserve the commutation relations of the input-output dynamics [31, 32]. This rules out many possible transfer matrices, greatly reducing the problem of exploring the realisations of the most general input-output transfer matrices for a given number of degrees of freedom. We will consider the most general SISO transfer matrix, given by,

$$\begin{bmatrix} \hat{y}_1(\Omega) \\ \hat{y}_2(\Omega) \end{bmatrix} = \begin{bmatrix} G_{11}(\Omega) & 0 \\ 0 & G_{22}(\Omega) \end{bmatrix} \begin{bmatrix} \hat{u}_1(\Omega) \\ \hat{u}_2(\Omega) \end{bmatrix}, \quad (8)$$

where $\hat{y}_{1,2}$ and $\hat{u}_{1,2}$ are the output and input fields respectively in the two-photon quadrature formalism [28, 29]. We choose the off-diagonal rotation terms to be zero without loss of generality. One special case is where $|G_{11}(\Omega)|^2 = |G_{22}(\Omega)|^2 = 1$ in which case we have no squeezing (see Section. VI). To parameterise the transfer function we consider an n degree-of-freedom pole-zero form,

$$G_{11}(\Omega) = \frac{\prod_{j=1}^n (i\Omega - z_j)}{\prod_{k=1}^n (i\Omega - p_k)}, \quad (9)$$

where $\{z_j \in \mathbb{C} | j = 1, \dots, n\}$, $\{p_k \in \mathbb{C} | k = 1, \dots, n\}$ are the zeroes and poles respectively, and n is equal to the number of internal modes of the minimal realization. As shown in [32] the transfer matrix is physically realisable if,

$$\mathbf{G}_q^\dagger(-\Omega^*) \Theta \mathbf{G}_q(-\Omega) = \Theta, \quad (10)$$

and,

$$\Theta = \begin{bmatrix} 0 & i \\ -i & 0 \end{bmatrix}. \quad (11)$$

This condition restricts the conjugate transfer function to,

$$G_{22}(\Omega) = \frac{\prod_{k=1}^n (-i\Omega - p_k^*)}{\prod_{j=1}^n (-i\Omega - z_j^*)}, \quad (12)$$

and so the poles/zeroes of G_{22} are the conjugates of the zeroes/poles of G_{11} respectively and the sign of the frequency is flipped. Since the real and imaginary parts of the poles and zeroes are independent we have in total $4n$ independent parameters specifying our system.

The possible poles and zeroes can be further reduced by noting that the quadrature operators are real in the time-domain and so the transfer matrix must obey $\mathbf{G}_q(-\Omega) = \mathbf{G}_q^\dagger(\Omega)$, which leads to the equation,

$$\prod_{j,k=1}^n (-i\Omega - p_k)(i\Omega - z_j^*) = \prod_{j,k=1}^n (i\Omega - p_k^*)(-i\Omega - z_j), \quad (13)$$

which can be expanded as,

$$\sum_{j=1}^{2n} a_j (i\Omega)^{j-1} = 0, \quad (14)$$

where a_j are algebraic combinations of the poles and zeroes. Therefore we have $a_j = 0$, $j = 1, \dots, 2n$ and the number of independent parameters is reduced to $2n$.

V. INTERNAL SQUEEZING

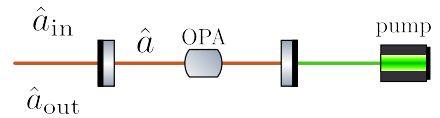


FIG. 1. The setup for the squeezing of one quadrature via internal squeezing within the cavity, achieving an SNR that diverges at DC. The OPA (optical parametric amplifier) is pumped by the classical pump beam.

In this section we consider the minimal realisation of a general first-order input-output transfer matrix exhibiting squeezing, i.e. $|G(\Omega)| \neq 1$ for the quadrature operators, and the off-diagonal terms are non-zero for the

sideband operators. We will see that the internal squeezing schemes saturate the Heisenberg limit. According to the previous section, the most general first-order transfer matrix is quantified by two independent real parameters, and is given in the quadrature picture by,

$$\mathbf{G}^q(\Omega) = \begin{bmatrix} \frac{\alpha+i\Omega}{\beta-i\Omega} & 0 \\ 0 & \frac{\beta+i\Omega}{\alpha-i\Omega} \end{bmatrix}, \quad (15)$$

which obeys Eq. (10). In Appendix. B we derive the physically realisable state-space directly from the above transfer matrix giving,

$$A = \frac{1}{2} \begin{bmatrix} -\alpha - \beta & \alpha - \beta \\ \alpha - \beta & -\alpha - \beta \end{bmatrix}, \quad (16)$$

$$B = \sqrt{\alpha + \beta} I_{2 \times 2},$$

$$C = -\sqrt{\alpha + \beta} I_{2 \times 2}, \quad D = I_{2 \times 2}.$$

The physical realisation of this system has one internal degree of freedom and in the generalized open oscillator formalism (discussed extensively in [26]) is given by,

$$S = I_{2 \times 2} \quad (17)$$

$$\hat{L} = \sqrt{\alpha + \beta} \hat{a} \quad (18)$$

$$\hat{H} = -\frac{i}{4} \hbar (\alpha - \beta) (\hat{a} \hat{a} - \hat{a}^\dagger \hat{a}^\dagger), \quad (19)$$

where \hat{a} is the annihilation operator of the cavity mode. Here S is the input-output direct scattering matrix, \hat{L} is the coupling operator to the external continuum, and finally \hat{H} is the system's internal Hamiltonian in the rotating frame at the laser carrier frequency. As shown in [22] this corresponds to a tuned cavity with coupling coefficient $\gamma \equiv (\alpha + \beta)/2$ containing a non-linear crystal with coupling frequency $\chi \equiv (\alpha - \beta)/2$, which is related to the single-pass squeezing factor by $r = 2\chi L/c$ where L is the cavity length. Inverting these relations gives $\alpha = \gamma + \chi$ and $\beta = \gamma - \chi$.

The quadrature picture transfer matrix from the inputs to the internal degree of freedom is given by,

$$\begin{bmatrix} \hat{a}^1 \\ \hat{a}^2 \end{bmatrix} = \begin{bmatrix} \frac{\sqrt{2\gamma}}{\gamma - \chi - i\Omega} & 0 \\ 0 & \frac{\sqrt{2\gamma}}{\gamma + \chi - i\Omega} \end{bmatrix} \begin{bmatrix} \hat{a}_{\text{in}}^1 \\ \hat{a}_{\text{in}}^2 \end{bmatrix}. \quad (20)$$

In this case, the probe degree of freedom is proportional to the probe amplitude quadrature \hat{a}^1 . Fixing the proportional constant (the actual value does not affect the optimisation), we have $\hat{F} \equiv (\hbar\omega_0\sqrt{2N}/L)\hat{a}^1$ with N the mean photon number and the input field is $\hat{u} \equiv \hat{a}_{\text{in}}^1$ giving the input-to-probe transfer function,

$$G_{uF}(\Omega) = \left(\frac{\hbar\omega_0\sqrt{2N}}{L} \right) \frac{\sqrt{2\gamma}}{\gamma - \chi - i\Omega}. \quad (21)$$

The probe photon fluctuation is given by the integral in Eq. (7),

$$\sigma_{NN} = 2N \int_0^\infty \frac{d\Omega}{2\pi} \frac{2\gamma}{|\gamma - \chi - i\Omega|^2}. \quad (22)$$

Clearly at $\gamma = \chi$ the integrand diverges at $\Omega = 0$ and thus the total probe fluctuation will diverge, and the Heisenberg limit will be saturated. This corresponds to the threshold case where the cavity acts as an optical parametric oscillator, since the damping of the cavity mode exactly compensates the pumping due to the non-linear crystal interaction. At $\gamma \neq \chi$ the integral is solved trivially as,

$$\sigma_{NN} = \frac{N\gamma}{|\gamma - \chi|}, \quad (23)$$

which is shot noise limited at $\chi = 0$, i.e. at no internal squeezing, but can be made to surpass it for $\chi > 0$. We have therefore recovered the internal squeezing approach to enhancing the quantum-limited sensitivity previously developed in [17–19].

In Appendix. C we demonstrate this approach starting with a second-order transfer matrix, arriving again at an internal squeezing design, with the same condition $\gamma = \chi$ resulting in a divergent response.

VI. REALISATION OF QND VIA SIGNAL AMPLIFICATION

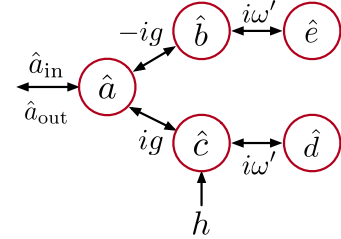


FIG. 2. A schematic representation of the most complex realisation developed in Section. VI. The modes \hat{b} and \hat{c} are coupled to the mode \hat{a} via a squeezing-like interaction and beamsplitter-like interaction respectively with the same coupling frequency g , with the signal h being coupled to mode \hat{c} . In this setup the signal response diverges at DC. We then add two additional modes \hat{d} and \hat{e} coupled to the modes \hat{b} and \hat{c} respectively, both via beamsplitter-like couplings with coupling frequency ω' which shifts the signal response resonance to $\Omega = \omega'$.

In this section we will consider the non-minimal realisation of the general first-order system, showing that the Heisenberg limit can be saturated with the addition of hidden internal modes that internally amplify the signal. We will first show that the minimal realization of a first-order system without squeezing is constrained by the Mizuno limit [33], and use the recent discovery that an infinite DC signal response can be achieved by adding a pair of modes that do not manifest in the input-output dynamics [20] and thus do not add any additional noise. We will show how this is the simplest case of a general class of such non-minimal realisations, and that a quantum-mechanics-free subspace is formed allowing for

arbitrary modification of the system dynamics. By asserting that the input-output behaviour remain the same, we have internal signal amplification without adding additional noise channels.

First, considering the case of Eq. (15) without squeezing with $\alpha = \beta \equiv \gamma$, the physically realisable state-space is given by,

$$\mathbf{G}^q(\Omega) = \begin{bmatrix} \frac{\Omega - i\gamma}{\Omega + i\gamma} & 0 \\ 0 & \frac{\Omega - i\gamma}{\Omega + i\gamma} \end{bmatrix}. \quad (24)$$

The corresponding generalized open oscillator is given by,

$$S = I_{2 \times 2}, \quad \hat{L} = -\sqrt{2\gamma}\hat{a}, \quad \hat{H} = 0, \quad (25)$$

and the corresponding minimal realization is a simple tuned cavity where γ is the cavity bandwidth. We can express the dynamics in the sideband picture by the Langevin equation and associated input-output relation, [34–37]

$$\dot{\hat{a}} = -\gamma\hat{a} + \sqrt{2\gamma}\hat{a}_{\text{in}} \quad (26)$$

$$\hat{a}_{\text{out}} = \hat{a}_{\text{in}} - \sqrt{2\gamma}\hat{a}. \quad (27)$$

The transfer function from the input vacuum to the amplitude quadrature is given by,

$$G_{uF}(\Omega) = \frac{\sqrt{2\gamma}}{\gamma - i\Omega}. \quad (28)$$

Integrating this over all frequencies gives 2π and thus the total SNR will be bounded by a constant independent of the bandwidth, which is the aforementioned Mizuno limit. Specifically, the detector is limited by the shot noise limit $\sigma_{NN} = N$ where N is the average photon number, giving $\text{SNR} = \omega_0^2 N^2 / 2 = E^2 / (2\hbar^2)$ where E is the average energy. Generally passive resonant detectors exhibit such a limit: dependent on the average stored energy, but independent of the parameters.

We now consider adding two auxiliary modes \hat{b} and \hat{c} as shown in Fig. 2 and discussed in [20], without modifying the input-output dynamics. In Appendix. D we derive a general approach by which such hidden auxiliary modes can be added. The general condition is given by,

$$\begin{aligned} T^{(a)}(\Omega) &\equiv \begin{bmatrix} ig_b & -ig_{b^\dagger} \\ ig_{b^\dagger}^* & -ig_b^* \end{bmatrix} T^{(b)}(\Omega) \\ &+ \begin{bmatrix} ig_c & -ig_{c^\dagger} \\ ig_{c^\dagger}^* & -ig_c^* \end{bmatrix} T^{(c)}(\Omega) = 0. \end{aligned} \quad (29)$$

where $T^{(b)}(\Omega)$ and $T^{(c)}(\Omega)$ are transfer matrices given in Eq. (D15) and (D16) respectively, and the most general linear Hamiltonian with two extra possibly-hidden modes is given by,

$$\begin{aligned} &-\hbar g_b(\hat{a}\hat{b}^\dagger + \hat{a}^\dagger\hat{b}) - \hbar g_{b^\dagger}(\hat{a}\hat{b} + \hat{a}^\dagger\hat{b}^\dagger) \\ &-\hbar g_c(\hat{a}\hat{c}^\dagger + \hat{a}^\dagger\hat{c}) - \hbar g_{c^\dagger}(\hat{a}\hat{c} + \hat{a}^\dagger\hat{c}^\dagger). \end{aligned}$$

The terms with coupling rates g_b and g_c are coupled to \hat{a} via a beamsplitter, and the terms with coupling rates g_{b^\dagger} and g_{c^\dagger} via a non-linear crystal (or equivalently an optomechanical interaction with optomechanical coupling frequency g , as discussed in [12, 20]). Each auxiliary mode has just one degree of freedom, and thus the transfer matrices are given by,

$$T^{(b)}(\Omega) = \frac{1}{-i\Omega} \begin{bmatrix} ig_b & -ig_{b^\dagger} \\ ig_{b^\dagger}^* & -ig_b^* \end{bmatrix}, \quad (30)$$

$$T^{(c)}(\Omega) = \frac{1}{-i\Omega} \begin{bmatrix} ig_c & -ig_{c^\dagger} \\ ig_{c^\dagger}^* & -ig_c^* \end{bmatrix}. \quad (31)$$

This gives,

$$T^{(a)}(\Omega) \equiv \frac{1}{-i\Omega} (-g_b^2 + g_{b^\dagger}^2 - g_c^2 + g_{c^\dagger}^2) I_{2 \times 2}. \quad (32)$$

If we now choose cavity mode \hat{c} to be coupled to mode \hat{a} purely by a beamsplitter-like interaction, then we have $g_c = \omega_s$ with ω_s being the sloshing frequency between the mode \hat{c} and mode \hat{a} and no non-linear coupling: $g_{c^\dagger} = 0$. Therefore the input-output dynamics are left invariant if $g_b = 0$ and $g_{b^\dagger} = \omega_s$, and so mode \hat{b} should be coupled to mode \hat{a} via a non-linear interaction (e.g. a non-linear crystal if \hat{b} is an optical mode) with the same coupling constant as the \hat{c} mode: $g \equiv g_{b^\dagger} = \omega_s$. The most general Hamiltonian with two hidden modes is thus given by,

$$\hat{H}_0 = -\hbar g(\hat{a}\hat{c}^\dagger + \hat{a}^\dagger\hat{c}) - \hbar g(\hat{a}\hat{b} + \hat{a}^\dagger\hat{b}^\dagger). \quad (33)$$

Such a system is known as being PT(parity-time)-symmetric as the Hamiltonian is invariant under the parity operation (reversing modes \hat{c} and \hat{b} via $\hat{c} \leftrightarrow \hat{b}^\dagger$, $\hat{c}^\dagger \leftrightarrow \hat{b}$) together with the time reversal operation ($\hat{c} \leftrightarrow \hat{c}^\dagger$, $\hat{b} \leftrightarrow \hat{b}^\dagger$) [38]. The equations of motion are given by,

$$\dot{\hat{a}} = -\gamma\hat{a} + ig\hat{c} + ig\hat{b}^\dagger + \sqrt{2\gamma}\hat{a}_{\text{in}}, \quad (34)$$

$$\dot{\hat{b}}^\dagger = -ig\hat{a}, \quad (35)$$

$$\dot{\hat{c}} = ig\hat{a}. \quad (36)$$

In this case, we have the probe degree of freedom proportional to the amplitude quadrature of the \hat{c} mode cavity $\hat{F} \propto (\hat{c} + \hat{c}^\dagger)/\sqrt{2}$ and the input as the amplitude quadrature $\hat{u} = (\hat{a}_{\text{in}} + \hat{a}_{\text{in}}^\dagger)/\sqrt{2}$. Solving in the frequency domain we can find the input-to-probe transfer function,

$$G_{uF}(\Omega) \propto \frac{g}{\Omega} \frac{\sqrt{2\gamma}}{\gamma - i\Omega}, \quad (37)$$

and therefore the probe fluctuation S_{FF} diverges at DC and thus σ_{NN} diverges and the Heisenberg limit is saturated.

We can show that the diverging probe fluctuation occurs due to the setup realising an ideal QND (quantum non-demolition) measurement [23], in which case the probe degree of freedom has infinite fluctuation as

it is conjugate to a conserved QND quantity. Re-writing Eq. (33),

$$\hat{H}_0 = -\hbar g[\hat{a}^\dagger(\hat{c} + \hat{b}^\dagger) + \hat{a}(\hat{c}^\dagger + \hat{b})], \quad (38)$$

it can be seen that the composite quantity $\hat{c} + \hat{b}^\dagger$ is conserved, since

$$\frac{d}{dt}(\hat{c} + \hat{b}^\dagger) \propto [\hat{c} + \hat{b}^\dagger, \hat{c}^\dagger + \hat{b}] = 0. \quad (39)$$

This further implies two conserved quantities $\hat{X}_+ \equiv (\hat{X}_c + \hat{X}_b)/\sqrt{2}$, $\hat{Y}_- \equiv (\hat{Y}_c - \hat{Y}_b)/\sqrt{2}$ in terms of amplitude and phase quadratures $\hat{X}_c \equiv (\hat{c} + \hat{c}^\dagger)/\sqrt{2}$, $\hat{Y}_c \equiv (\hat{c} - \hat{c}^\dagger)/\sqrt{2}i$ (and similarly for \hat{a} and \hat{b}). Additionally we also define $\hat{X}_- \equiv (\hat{X}_c - \hat{X}_b)/\sqrt{2}$. Rewriting the Hamiltonian in terms of these quantities gives,

$$\hat{H}_0 = \hbar g(\hat{Y}_a \hat{X}_+ - \hat{X}_b \hat{Y}_-) - \hbar(\alpha/\sqrt{2})(\hat{X}_+ + \hat{X}_-)h, \quad (40)$$

The relevant residue part leading to detection of the signal h reads:

$$\hat{H}_{\text{res}} = -\hbar g \hat{X}_a \hat{Y}_- - \hbar(\alpha/\sqrt{2}) \hat{X}_- h, \quad (41)$$

with \hat{Y}_- being the conserved QND observable and \hat{X}_- being the probe degree-of-freedom thus having infinite variance and therefore giving infinite signal response. In frequency-domain, \hat{Y}_- exhibits the divergence at DC:

$$\hat{Y}_-(\Omega) = \frac{i\alpha}{\sqrt{2}\Omega} h(\Omega). \quad (42)$$

As discovered above, the operators \hat{X}_+ and \hat{Y}_- are constants of motion and therefore act form a quantum-mechanics-free subsystem [25]. The dynamics can be arbitrarily modified while keeping this subsystem quantum-mechanics-free so long as the simultaneous measurability condition is kept,

$$[\hat{X}_+(t), \hat{X}_+(t')] = [\hat{Y}_-(t), \hat{Y}_-(t')] = 0. \quad (43)$$

We can then modify the dynamics such that the Heisenberg limit is saturated over a range of frequencies. As an example, we can shift the divergent response from DC to another frequency ω' by adding an extra pair of modes \hat{d} and \hat{e} which couple to \hat{b} and \hat{c} respectively. In this case the interaction Hamiltonian gains the following terms,

$$\begin{aligned} & -\hbar\omega'(\hat{b}\hat{d}^\dagger + \hat{b}^\dagger\hat{d} + \hat{c}^\dagger\hat{e} + \hat{c}\hat{e}^\dagger) \\ & = i\hbar\omega'(\hat{X}_+ \hat{Q}_+ + \hat{Y}_+ \hat{P}_+ - \hat{Y}_- \hat{P}_- + \hat{X}_- \hat{Q}_-), \end{aligned}$$

which satisfies the general condition given in Eq. (29) and thus does not affect the input-output dynamics, and where we have defined,

$$\hat{Q}_\pm \equiv \frac{\hat{X}_d \pm \hat{X}_e}{\sqrt{2}}, \quad \hat{P}_\pm \equiv \frac{\hat{Y}_d \pm \hat{Y}_e}{\sqrt{2}}. \quad (44)$$

The residue part relevant to signal detection gains the term,

$$\hbar\omega'(\hat{X}_- \hat{Q}_- - \hat{Y}_- \hat{P}_-). \quad (45)$$

The latter term modifies the dynamics of \hat{Y}_- to become,

$$\dot{\hat{Y}}_- = -\omega' \hat{Q}_- + \frac{\alpha}{\sqrt{2}} h, \quad (46)$$

$$\dot{\hat{Q}}_- = \omega' \hat{Y}_-, \quad (47)$$

and so eliminating \hat{Q}_- in the frequency domain we obtain,

$$\hat{Y}_-(\Omega) = \frac{i\alpha\Omega}{\sqrt{2}(\Omega^2 - \omega'^2)} h(\Omega). \quad (48)$$

We see that the signal response now diverges at $\Omega = \omega'$ rather than at DC, and that the PT symmetric case shown in Eq. (42) is recovered for $\omega' = 0$. The final phase quadrature input-output relation is given by,

$$\hat{Y}_{\text{out}}(\Omega) = -\frac{\Omega - i\gamma}{\Omega + i\gamma} \hat{Y}_{\text{in}}(\Omega) + \frac{\sqrt{\gamma}\alpha g \Omega h(\Omega)}{(\Omega^2 - \omega'^2)(\Omega + i\gamma)}, \quad (49)$$

and so via the divergent signal amplification we now have an infinite signal response at a chosen frequency.

VII. DISCUSSION

We have demonstrated a systematic method for constructing detectors that saturate the Heisenberg limit, specifically investigating the first-order transfer matrix. Investigating minimal realisations, we showed that those that saturate the Heisenberg limit are internal squeezing designs. Considering non-minimal realisations, we investigated PT symmetric systems and showed that such systems realise a general QND measurement and saturate the Heisenberg limit, further showing how their dynamics can be modified without losing this property.

Another further exploration will be a systematic realisation of the transmission-readout setup presented in [12], however this requires systematically realising a 4×4 MIMO (multi-input multi-output) transfer matrix with third order elements, which will be complicated to realise directly using the aforementioned framework. Further, we can consider experimental demonstrations of the aforementioned PT-symmetric setups. Optomechanical realisations are currently in development, however there is also the open possibility for an all-optical demonstration that avoids the strict thermal noise requirements expected in the optomechanical design. Finally, we should also extend the analysis to take optical losses into account, potentially developing methods for optimising the design so that they have a minimal impact on the SNR.

VIII. ACKNOWLEDGEMENTS

We would like to thank Denis Martynov, LIGO AIC, and QNWG for fruitful discussions. J.B. is supported by STFC and School of Physics and Astronomy at the University of Birmingham. J.B. and H.M. acknowledge the additional support from the Birmingham Institute for Gravitational Wave Astronomy. H.M. has also been supported by UK STFC Ernest Rutherford Fellowship (Grant No. ST/M005844/11). Y.C. is supported by the Simons Foundation (Award Number 568762), and the National Science Foundation, through Grants PHY-1708212 and PHY-1708213.

Appendix A: Linear Systems

The general solution for \mathbf{x} and \mathbf{y} of the linear system (1) is:

$$\begin{aligned}\mathbf{x}(t) &= e^{At}\mathbf{x}(0-) + \int_{0-}^t e^{A(t-\tau)}B\mathbf{u}(\tau)d\tau, \\ \mathbf{y}(t) &= Ce^{At}\mathbf{x}(0-) + \int_{0-}^t Ce^{A(t-\tau)}B\mathbf{u}(\tau)d\tau + D\mathbf{u}(t).\end{aligned}$$

Taking the initial condition to be at $t = 0^-$ allows the consideration of impulse inputs $\delta(t)$ and a step discontinuity in \mathbf{x} from $t = 0^-$ to $t = 0^+$ (the time just after $t = 0$).

The system is asymptotically stable if the matrix A is Hurwitz, that is, all its eigenvalues have a real part < 0 . In an asymptotically stable system, the natural response asymptotically decays to zero, $\lim_{t \rightarrow \infty} e^{At}\mathbf{x}(0-) = 0$ for any initial condition $\mathbf{x}(0^-)$. The impulse response h for an asymptotically stable system also decays to 0 as $t \rightarrow \infty$.

For a sinusoid input $\mathbf{u}(t) = \mathbf{b}(\Omega)e^{-i\Omega t}$, where Ω is real and $\mathbf{b}(\Omega)$ is a fixed column vector of operators (in our case this vector contains the quantized modes of an input quantum field), the asymptotic output as $t \rightarrow \infty$ of an asymptotically stable system only has the forced response and is given by:

$$\mathbf{y}(t) = H(\Omega)\mathbf{b}(\Omega)e^{-i\Omega t}, \quad (\text{A1})$$

where $H(\Omega)$ is as given in (2) with $\sigma \geq 0$. In this case, H coincides with the Fourier transform of h and is called the system's frequency response. For an input $\mathbf{u}(t) = \int_{-\infty}^{\infty} \mathbf{b}(\Omega)e^{-i\Omega t}d\Omega$, by linearity of the system the asymptotic response is $\mathbf{y}(t) = \int_{-\infty}^{\infty} H(\Omega)\mathbf{b}(\Omega)e^{-i\Omega t}d\Omega$.

For a system that is not asymptotically stable, the impulse response may not be integrable, $\int_{0-}^{\infty} |h(t)|dt = \infty$, and the frequency response H not well-defined. For such systems, the forced response to a sinusoid input may not have an asymptotic solution. However, for $h(t) = O(e^{\sigma t})$, with $\sigma \geq 0$, it can have an asymptotic solution for inputs of the form $\mathbf{u}(t) = \mathbf{b}(\Omega)e^{-i\Omega t}$ for all complex Ω with $\Im\{\Omega\} > \sigma$ and with $\mathbf{b}(\Omega)$ some fixed

vector of operators as before. In this case, the asymptotic forced response is again given by the right hand side of (A1) but Ω is now complex. For more general inputs of the form $\mathbf{u}(t) = \int_{-\infty}^{\infty} \mathbf{b}(\omega + i\sigma_0)e^{-i(\omega + i\sigma_0)t}d\omega$, with $\sigma_0 > \sigma$, by linearity the forced response is given by $\mathbf{y}_f(t) = \int_{-\infty}^{\infty} H(\omega + i\sigma_0)\mathbf{b}(\omega + i\sigma_0)e^{-i(\omega + i\sigma_0)t}d\omega$.

Appendix B: Physically Realisable State-space for Internal Squeezing

We will now follow the steps given in [22] to systematically construct the physically realisable state space of the internal squeezing setup whose transfer matrix is shown in Eq. 15. First we define a de-dimensionalised frequency with respect to α by making the transformation $\Omega \rightarrow \alpha\Omega$, so that the aforementioned transfer matrix becomes,

$$\mathbf{G}^q(\Omega) = \begin{bmatrix} \frac{1+i\Omega}{\Gamma-i\Omega} & 0 \\ 0 & \frac{\Gamma+i\Omega}{1-i\Omega} \end{bmatrix}, \quad (\text{B1})$$

where $\Gamma \equiv \beta/\alpha$. Assuming that the amplitude quadrature is squeezed, i.e. $\Gamma < 1$, we can compute the canonical state-space realisation using Mathematica,

$$A' = \frac{1}{3 + \gamma^2} \begin{bmatrix} -(1 + \Gamma)^2 & c_1 \\ c_1 & -2 - \Gamma - \Gamma^3 \end{bmatrix}, \quad (\text{B2})$$

$$B' = \begin{bmatrix} 0 & \sqrt{\frac{2}{3 + \Gamma^2}} \\ \frac{1}{2}\sqrt{\frac{3 + \Gamma^2}{1 + \Gamma^2}} & \frac{\Gamma^2 - 1}{2\sqrt{3 + 4\Gamma^2 + \Gamma^4}} \end{bmatrix}, \quad (\text{B3})$$

$$C' = \begin{bmatrix} \frac{(1 + \Gamma)^2|\Gamma - 1|}{\sqrt{2(3 + \Gamma^2)}} & \frac{2(1 + \Gamma)(1 + \Gamma^2)}{\sqrt{3 + 4\Gamma^2 + \Gamma^4}} \\ (1 + \Gamma)\sqrt{\frac{3 + \Gamma^2}{2}} & 0 \end{bmatrix}, \quad (\text{B4})$$

$$D' = -I_{2 \times 2}. \quad (\text{B5})$$

where $c_1 = \sqrt{2}\sqrt{1 + \Gamma^2}|\Gamma - 1|$ and $I_{2 \times 2}$ is the 2×2 identity matrix. This state-space does not currently fulfil the physical realisability condition, given by, [22]

$$AJ + JA^\dagger + BJB^\dagger = 0, \quad (\text{B6})$$

$$JC^\dagger + BJD^\dagger = 0, \quad (\text{B7})$$

where,

$$J = \begin{bmatrix} 1 & 0 \\ 0 & -1 \end{bmatrix}. \quad (\text{B8})$$

To find the transformation from the unrealisable state-space (A', B', C', D') to the realisable state-space (A, B, C, D) we look for the matrix X that satisfies,

$$A'X + X(A')^\dagger + B'J(B')^\dagger = 0, \quad (\text{B9})$$

$$X(C')^\dagger + B'J(D')^\dagger = 0. \quad (\text{B10})$$

In this case one such matrix is given by,

$$X = \begin{bmatrix} -\frac{2}{3 + 3\Gamma + \Gamma^2 + \Gamma^3} & \frac{\sqrt{3 + 4\Gamma^2 + \Gamma^4}|\Gamma - 1|}{\sqrt{2(1 + \Gamma^2)}(3 + \Gamma^2)^{3/2}} \\ \frac{1 - \Gamma}{\sqrt{2(1 + \Gamma^2)}(3 + \Gamma^2)} & \frac{2}{3 + 3\Gamma + \Gamma^2 + \Gamma^3} \end{bmatrix}. \quad (\text{B11})$$

We then look for the similarity transformation matrix T satisfying $X = TJT^\dagger$, which in this case is given by,

$$T = \begin{bmatrix} 0 & \sqrt{\frac{2}{3+3\Gamma+\Gamma^2+\Gamma^3}} \\ \frac{1}{2}\sqrt{\frac{3+\Gamma^2}{1+\Gamma+\Gamma^2+\Gamma^3}} & \frac{\Gamma^2-1}{2\sqrt{(1+\Gamma^2)(3+3\Gamma+\Gamma^2+\Gamma^3)}} \end{bmatrix}. \quad (\text{B12})$$

We can apply this transformation by the standard state-space transformation,

$$A = T^{-1}A'T, \quad B = T^{-1}B', \quad C = C'T, \quad D = D', \quad (\text{B13})$$

which gives the state-space,

$$A = \frac{1}{2} \begin{bmatrix} -1-\Gamma & 1-\Gamma \\ -1+\Gamma & -1-\Gamma \end{bmatrix}, \quad (\text{B14})$$

$$B = \sqrt{1+\Gamma}I_{2 \times 2}, \quad (\text{B15})$$

$$C = \sqrt{1+\Gamma}I_{2 \times 2}, \quad (\text{B16})$$

$$D = -I_{2 \times 2}. \quad (\text{B17})$$

To slightly simplify the physical realisation without loss of generality we can add a π phase shift for the input-output reflection, resulting in transforming the state space via $C \rightarrow -C$ and $D \rightarrow -D$. Substituting $\Gamma = \beta/\alpha$ and reversing the de-dimensionalisation via $\Omega \rightarrow \Omega/\alpha$ we obtain the physically realisable state-space which obeys Eqs. (B6) and (B7),

$$A = \frac{1}{2} \begin{bmatrix} -\alpha-\beta & \alpha-\beta \\ \alpha-\beta & -\alpha-\beta \end{bmatrix}, \quad (\text{B18})$$

$$B = \sqrt{\alpha+\beta} I_{2 \times 2},$$

$$C = -\sqrt{\alpha+\beta} I_{2 \times 2}, \quad D = I_{2 \times 2}.$$

Appendix C: Quantum Expander

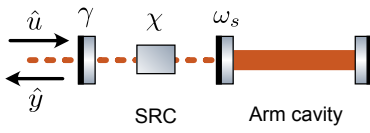


FIG. 3. The setup analysed for the quantum expander as explored in [19], equivalent to a tuned Michelson interferometer except with squeezing (via a non-linear crystal) internally within the SRC (signal recycling cavity).

In this appendix we consider the general second-order input-output transfer matrix, showing that the optimal sensitivity is achieved when the parameters match that of the so-called quantum expander first explored in [19], a setup which, similarly to the transmission-readout setup discussed in [12], can directly increase the detection bandwidth of a gravitational-wave interferometer. This setup, shown in Figure. 3, consists of a tuned, signal-recycled Michelson interferometer with internal squeezing in the signal recycling cavity. The signal-recycled

Michelson can be mapped to an equivalent coupled-cavity [39]. We show that the quantum expander is the optimal detector for any second-order quadrature-picture transfer matrix obeying the constraints in Section. IV.

Thus we start with the most general proper second-order input-output transfer matrix,

$$\mathbf{G}^q(\Omega) = \begin{bmatrix} \frac{(i\Omega-\alpha_1)(i\Omega-\beta_1)}{(i\Omega-\alpha_2)(i\Omega-\beta_2)} & 0 \\ 0 & \frac{(-i\Omega-\alpha_2)(-i\Omega-\beta_2)}{(-i\Omega-\alpha_1)(-i\Omega-\beta_1)} \end{bmatrix}, \quad (\text{C1})$$

where $\alpha_1, \alpha_2, \beta_1, \beta_2 \in \mathbb{R}$. Requiring that there is no gain at DC we also obtain the condition $\alpha_1\beta_1 = \alpha_2\beta_2$. We then follow the same procedure as in Appendix. B for finding the physically realisable state-space, obtaining,

$$\begin{aligned} A &= \begin{bmatrix} 0 & 0 & -i\omega_s & 0 \\ 0 & 0 & 0 & i\omega_s \\ -i\omega_s & 0 & -\gamma & -\chi \\ 0 & i\omega_s & -\chi & -\gamma \end{bmatrix}, \\ B &= \begin{bmatrix} 0 & 0 \\ 0 & 0 \\ \sqrt{2}\sqrt{\gamma} & 0 \\ 0 & \sqrt{2}\sqrt{\gamma} \end{bmatrix}, \\ C &= \begin{bmatrix} 0 & 0 & -\sqrt{2}\sqrt{\gamma} & 0 \\ 0 & 0 & 0 & -\sqrt{2}\sqrt{\gamma} \end{bmatrix}, \quad D = I_{2 \times 2}, \end{aligned} \quad (\text{C2})$$

where $\gamma \equiv \frac{1}{2}(-\alpha_1 + \alpha_2 - \beta_1 + \beta_2)$, $\chi \equiv \frac{1}{2}(\alpha_1 + \alpha_2\beta_1 + \beta_2)$, and $\omega_s \equiv \sqrt{\alpha_1\beta_1}$. This corresponds to the dynamics derived from Hamiltonian for the quantum expander first described in [19]. In this case since we have a two degree-of-freedom we have to apply the separation theorem of [26] to separate it into two separated one degree-of-freedom systems. The corresponding quantum network is given by $\mathcal{N} = \{\{G_1, G_2\}, \hat{H}^d, \mathcal{S}\}$ where $\mathcal{S} = G_2 \triangleleft G_1$ represents the series product [40], i.e. the output of G_1 is fed into G_2 . The two generalized open oscillators are given by,

$$G_1 = (I_{2 \times 2}, 0, 0), \quad (\text{C3})$$

$$G_2 = \left(I_{2 \times 2}, -\sqrt{2}\gamma\hat{a}_q, \frac{i}{2}\hbar\chi(\hat{a}_q\hat{a}_q + \hat{a}_q^\dagger\hat{a}_q^\dagger) \right), \quad (\text{C4})$$

where $I_{2 \times 2}$ is the 2×2 identity matrix, γ is the coupling frequency of the continuum to the cavity mode described by annihilation operator \hat{a}_q , and χ is the strength of the non-linear interaction. The Hamiltonian coupling the two cavities is given by $\hat{H}^d = \hbar\omega_s(\hat{a}_q\hat{a}^\dagger + \hat{a}_q^\dagger\hat{a})$ where \hat{a} is the cavity mode of the second cavity, and is therefore a simple beamsplitter-like coupling between the two cavities. Note that G_1 is not coupled to the external continuum and therefore it is only coupled to G_2 via H^d . In total we have two tuned cavities coupled by a beamsplitter-like interaction, with the first cavity coupled to the external continuum and exhibiting internal squeezing, and have thus recovered the quantum expander realisation pictured in Fig. 3.

The quadrature transfer matrix from the input to the

arm cavity mode \hat{a} was found to be,

$$\begin{bmatrix} \hat{a}^1 \\ \hat{a}^2 \end{bmatrix} = \begin{bmatrix} 0 & \frac{\sqrt{2\gamma}\omega_s}{i\omega(\chi-\gamma)+\omega_s^2-\omega^2} \\ -\frac{\sqrt{2\gamma}\omega_s}{-i\omega(\gamma+\chi)+\omega_s^2-\omega^2} & 0 \end{bmatrix} \begin{bmatrix} \hat{a}_{\text{in}}^1 \\ \hat{a}_{\text{in}}^2 \end{bmatrix}. \quad (\text{C5})$$

Using Eq. (7) we see that the SNR for signal coupled to the amplitude quadrature is given by $2\pi\gamma/|\gamma-\chi|$, which diverges as $\chi \rightarrow \gamma$. At $\chi \gg \gamma$ the SNR approaches zero since the non-linear interaction totally depletes the amplitude quadrature fluctuations in the cavity. The SNR for the phase quadrature is given by $2\pi\gamma/(\gamma+\chi)$ which is maximal at $\chi = 0$ where it is equal to 2π and is thus constrained by the Mizuno limit.

For the signal recycling cavity mode \hat{a}_q , we also see the divergence at $\chi \rightarrow \gamma$, except that in this case the SNR for the phase quadrature diverges rather than the amplitude quadrature,

$$\begin{bmatrix} \hat{a}_q^1 \\ \hat{a}_q^2 \end{bmatrix} = \begin{bmatrix} -\frac{i\sqrt{2}\sqrt{\gamma}\omega}{-i\omega(\gamma+\chi)+\omega_s^2-\omega^2} & 0 \\ 0 & -\frac{i\sqrt{2}\sqrt{\gamma}\omega}{-i\omega(\chi-\gamma)+\omega_s^2-\omega^2} \end{bmatrix} \begin{bmatrix} \hat{a}_{\text{in}}^1 \\ \hat{a}_{\text{in}}^2 \end{bmatrix}. \quad (\text{C6})$$

In this case the SNR for the amplitude quadrature is given by $2\pi\gamma/(\gamma+\chi)$ and for the phase quadrature is given by $2\pi\gamma/|\gamma-\chi|$ i.e. the role of the amplitude and phase quadrature are swapped compared to the arm cavity mode.

Appendix D: Auxiliary Mode Dynamics.

In this section we will discuss how the dynamics of added auxiliary modes, shown in Fig. 2, can be inferred by requiring that the frequency-domain input-output relation remain unchanged by the addition of them. Each auxiliary mode is coupled to a set of n_d internal modes \hat{d}_j and n_e internal modes \hat{e}_j adding the following terms to the Hamiltonian,

$$\begin{aligned} & \sum_j -\hbar g_{d_j}(\hat{b}\hat{d}_j^\dagger + \hat{b}^\dagger\hat{d}_j) - \hbar g_{d_j^\dagger}(\hat{b}\hat{d}_j + \hat{b}^\dagger\hat{d}_j^\dagger) \\ & - \hbar g_{e_j}(\hat{c}\hat{e}_j^\dagger + \hat{c}^\dagger\hat{e}_j) - \hbar g_{e_j^\dagger}(\hat{c}\hat{e}_j + \hat{c}^\dagger\hat{e}_j^\dagger) \\ & + \sum_{i \neq j} \hbar g_{d_i d_j^\dagger}(\hat{d}_i\hat{d}_j^\dagger + \hat{d}_i^\dagger\hat{d}_j) + \hbar g_{d_i d_j}(\hat{d}_i\hat{d}_j + \hat{d}_i^\dagger\hat{d}_j^\dagger) \\ & + \sum_{i \neq j} \hbar g_{e_i e_j^\dagger}(\hat{e}_i\hat{e}_j^\dagger + \hat{e}_i^\dagger\hat{e}_j) + \hbar g_{e_i e_j}(\hat{e}_i\hat{e}_j + \hat{e}_i^\dagger\hat{e}_j^\dagger), \end{aligned}$$

where $g_{d_i d_j^\dagger}$ and $g_{d_i d_j}$ respectively quantify the beamsplitter-like and non-linear coupling between modes \hat{d}_i and \hat{d}_j , and similarly for the \hat{e} modes. Note that there is no direct coupling between the \hat{d} and \hat{e} modes.

The full set of equations of motion are,

$$\begin{aligned} \dot{\hat{a}} &= -\gamma\hat{a} + \sqrt{2\gamma}\hat{a}_{\text{in}} \\ & - ig_b\hat{b} + ig_{b^\dagger}\hat{b}^\dagger - ig_c\hat{c} + ig_{c^\dagger}\hat{c}^\dagger, \end{aligned} \quad (\text{D1})$$

$$\dot{\hat{b}} = ig_b\hat{a} - ig_{b^\dagger}\hat{a}^\dagger + i \sum_j g_{d_j}\hat{d}_j - i \sum_j g_{d_j^\dagger}\hat{d}_j^\dagger, \quad (\text{D2})$$

$$\dot{\hat{d}}_j = ig_{d_j}\hat{b} + ig_{d_j^\dagger}\hat{b}^\dagger - i \sum_{i \neq j} g_{d_i d_j^\dagger}\hat{d}_i - i \sum_{i \neq j} g_{d_i d_j}\hat{d}_i^\dagger, \quad (\text{D3})$$

$$\dot{\hat{c}} = ig_c\hat{a} - ig_{c^\dagger}\hat{a}^\dagger + i \sum_j g_{e_j}\hat{e}_j - i \sum_j g_{e_j^\dagger}\hat{e}_j^\dagger, \quad (\text{D4})$$

$$\dot{\hat{e}}_j = ig_{e_j}\hat{c} + ig_{e_j^\dagger}\hat{c}^\dagger - i \sum_{i \neq j} g_{e_i e_j^\dagger}\hat{e}_i - i \sum_{i \neq j} g_{e_i e_j}\hat{e}_i^\dagger. \quad (\text{D5})$$

Focussing on \hat{d}_j , the frequency-domain expression is given by,

$$-i\Omega\vec{d}(\Omega) = \vec{g}_d\hat{b}(\Omega) + \vec{g}_{d^\dagger}\hat{b}^\dagger(-\Omega) - iG\vec{d}(\Omega), \quad (\text{D6})$$

where,

$$\vec{g}_d = (ig_{d_1}, -ig_{d_1}^*, \dots, ig_{d_{n_d}}, -ig_{d_{n_d}}^*)^T, \quad (\text{D7})$$

$$\vec{g}_{d^\dagger} = (ig_{d_1}^\dagger, -ig_{d_1}^{\dagger*}, \dots, ig_{d_{n_d}}^\dagger, -ig_{d_{n_d}}^{\dagger*})^T, \quad (\text{D8})$$

and where,

$$\vec{d}(\Omega) = (\hat{d}_1(\Omega), \dots, \hat{d}_{n_d}(\Omega); \hat{d}_1^\dagger(-\Omega), \dots, \hat{d}_{n_d}^\dagger(-\Omega))^T. \quad (\text{D9})$$

and where in block form,

$$G^{(d)} = \begin{bmatrix} G_1^{(d)} \\ \vdots \\ G_{n_d}^{(d)} \end{bmatrix} \in \mathbb{C}^{2n_d \times 2n_d}, \quad (\text{D10})$$

where,

$$G_j^{(d)} = \begin{bmatrix} g_{d_1 d_j^\dagger} & \dots & g_{d_{n_d} d_j^\dagger} & g_{d_1 d_j} & \dots & g_{d_{n_d} d_j} \\ g_{d_1 d_j}^* & \dots & g_{d_{n_d} d_j}^* & g_{d_1 d_j}^\dagger & \dots & g_{d_{n_d} d_j}^\dagger \end{bmatrix}, \quad (\text{D11})$$

with $g_{d_j d_j} = g_{d_j d_j^\dagger} = 0$. Solving for $\vec{d}(\Omega)$ gives,

$$\begin{aligned} \vec{d}(\Omega) &= (-i\Omega I_{2n_d \times 2n_d} + iG^{(d)})^{-1} [\vec{g}_d \quad \vec{g}_{d^\dagger}] \begin{bmatrix} \hat{b}(\Omega) \\ \hat{b}^\dagger(-\Omega) \end{bmatrix} \\ &\equiv M^{(d)} \begin{bmatrix} \hat{b}(\Omega) \\ \hat{b}^\dagger(-\Omega) \end{bmatrix}, \end{aligned}$$

where $I_{2n_d \times 2n_d}$ is the $2n_d \times 2n_d$ identity matrix, and $M^{(d)} \in \mathbb{C}^{2n_d \times 2}$.

The frequency domain expression for \hat{b} is given by,

$$-i\Omega \begin{bmatrix} \hat{b}(\Omega) \\ \hat{b}^\dagger(-\Omega) \end{bmatrix} = \begin{bmatrix} ig_b & -ig_{b^\dagger} \\ ig_{b^\dagger}^* & -ig_b^* \end{bmatrix} \begin{bmatrix} \hat{a}(\Omega) \\ \hat{a}^\dagger(-\Omega) \end{bmatrix} + iD^{(d)}\vec{d}(\Omega), \quad (\text{D12})$$

where,

$$D^{(d)} = \begin{bmatrix} g_{d_1}, & \dots, & g_{d_{n_d}}; & -g_{d_1}^\dagger, & \dots, & -g_{d_{n_d}}^\dagger \\ g_{d_1}^*, & \dots, & g_{d_{n_d}}^*; & -g_{d_1}^*, & \dots, & -g_{d_{n_d}}^* \end{bmatrix}. \quad (\text{D13})$$

Solving for the \hat{b} mode we get,

$$\begin{bmatrix} \hat{b}(\Omega) \\ \hat{b}^\dagger(-\Omega) \end{bmatrix} = T^{(b)}(\Omega) \begin{bmatrix} \hat{a}(\Omega) \\ \hat{a}^\dagger(-\Omega) \end{bmatrix}, \quad (\text{D14})$$

where,

$$T^{(b)}(\Omega) \equiv (-i\Omega I_{2 \times 2} - iD^{(d)}M^{(d)})^{-1} \begin{bmatrix} ig_b & -ig_{b^\dagger} \\ ig_{b^\dagger}^* & -ig_b^* \end{bmatrix}, \quad (\text{D15})$$

and where $I_{2 \times 2}$ is the 2×2 identity matrix.

Similarly we have,

$$\begin{bmatrix} \hat{c}(\Omega) \\ \hat{c}^\dagger(-\Omega) \end{bmatrix} = T^{(c)}(\Omega) \begin{bmatrix} \hat{a}(\Omega) \\ \hat{a}^\dagger(-\Omega) \end{bmatrix},$$

where,

$$T^{(c)}(\Omega) \equiv (-i\Omega I_{2 \times 2} - iD^{(e)}M^{(e)})^{-1} \begin{bmatrix} ig_c & -ig_{c^\dagger} \\ ig_{c^\dagger}^* & -ig_c^* \end{bmatrix} \quad (\text{D16})$$

where,

$$D^{(e)} = \begin{bmatrix} g_{e_1}, & \dots, & g_{e_{n_e}}; & -g_{e_1}^\dagger, & \dots, & -g_{e_{n_e}}^\dagger \\ g_{e_1}^*, & \dots, & g_{e_{n_e}}^*; & -g_{e_1}^*, & \dots, & -g_{e_{n_e}}^* \end{bmatrix}, \quad (\text{D17})$$

and where,

$$M^{(e)} = (-i\Omega I_{2n_e \times 2n_e} + iG^{(e)})^{-1}, \quad (\text{D18})$$

where in block form,

$$G^{(e)} = \begin{bmatrix} G_1^{(e)} \\ \vdots \\ G_{n_e}^{(e)} \end{bmatrix} \in \mathbb{C}^{2n_e \times 2n_e}, \quad (\text{D19})$$

where,

$$G_j^{(e)} = \begin{bmatrix} g_{e_1 e_j}^\dagger & \dots & g_{e_{n_e} e_j}^\dagger; & g_{e_1 e_j} & \dots & g_{e_{n_e} e_j} \\ g_{e_1 e_j}^* & \dots & g_{e_{n_e} e_j}^*; & g_{e_1 e_j}^* & \dots & g_{e_{n_e} e_j}^* \end{bmatrix}. \quad (\text{D20})$$

The frequency domain expression for \hat{a} is given by,

$$\begin{aligned} -i\Omega \begin{bmatrix} \hat{a}(\Omega) \\ \hat{a}^\dagger(-\Omega) \end{bmatrix} &= \begin{bmatrix} ig_b & -ig_{b^\dagger} \\ ig_{b^\dagger}^* & -ig_b^* \end{bmatrix} \begin{bmatrix} \hat{b}(\Omega) \\ \hat{b}^\dagger(-\Omega) \end{bmatrix} \\ &+ \begin{bmatrix} ig_c & -ig_{c^\dagger} \\ ig_{c^\dagger}^* & -ig_c^* \end{bmatrix} \begin{bmatrix} \hat{c}(\Omega) \\ \hat{c}^\dagger(-\Omega) \end{bmatrix} + \dots, \\ &= T^{(a)}(\Omega) \begin{bmatrix} \hat{a}(\Omega) \\ \hat{a}^\dagger(-\Omega) \end{bmatrix} + \dots \end{aligned}$$

where \dots are the damping and input vacuum terms from Eq. (26) and where,

$$\begin{aligned} T^{(a)}(\Omega) &\equiv \begin{bmatrix} ig_b & -ig_{b^\dagger} \\ ig_{b^\dagger}^* & -ig_b^* \end{bmatrix} T^{(b)}(\Omega) \\ &+ \begin{bmatrix} ig_c & -ig_{c^\dagger} \\ ig_{c^\dagger}^* & -ig_c^* \end{bmatrix} T^{(c)}(\Omega) = 0. \end{aligned} \quad (\text{D21})$$

Therefore to keep the input-output dynamics invariant, all elements of this matrix must be zero.

-
- [1] C. Helstrom, Minimum mean-squared error of estimates in quantum statistics, *Physics Letters A* **25**, 101 (1967).
[2] V. B. Braginsky, Energetic quantum limit in large-scale interferometers, in *AIP Conference Proceedings*, Vol. 523 (AIP, 2000) pp. 180–190.
[3] A. Holevo, *Probabilistic and Statistical Aspects of quantum theory*, 2nd ed. (Scuola Normale Superiore, 2011).
[4] M. Tsang, H. M. Wiseman, and C. M. Caves, Fundamental quantum limit to waveform estimation, *Phys. Rev. Lett.* **106** (2011).
[5] H. Miao, R. X. Adhikari, Y. Ma, B. Pang, and Y. Chen, Towards the Fundamental Quantum Limit of Linear Measurements of Classical Signals, *Phys. Rev. Lett.* **119**, 050801 (2017).
[6] H. Miao, N. D. Smith, and M. Evans, Quantum Limit for Laser Interferometric Gravitational-Wave Detectors from Optical Dissipation, *Physical Review X* **9**, 11053 (2019).
[7] M. Zwiernik, C. A. Pérez-Delgado, and P. Kok, Ultimate limits to quantum metrology and the meaning of the Heisenberg limit, *Phys. Rev. A* **85**, 1 (2012).
[8] R. Schnabel, *Squeezed states of light and their applications in laser interferometers* (2017).
[9] G. S. Pati, M. Salit, K. Salit, and M. S. Shahriar, Demonstration of a tunable-bandwidth white-light interferometer using anomalous dispersion in atomic vapor, *Phys. Rev. Lett.* **99**, 133601 (2007).
[10] H. N. Yum, J. Scheuer, M. Salit, P. R. Hemmer, and M. S. Shahriar, Demonstration of white light cavity effect using stimulated Brillouin scattering in a fiber loop, *J. Lightwave Technol.* **31**, 3865 (2013).
[11] H. Miao, Y. Ma, C. Zhao, and Y. Chen, Enhancing the Bandwidth of Gravitational-Wave Detectors with Unstable Optomechanical Filters, *Phys. Rev. Lett.* **115**, 211104 (2015).
[12] J. Bentley, P. Jones, D. Martynov, A. Freise, and H. Miao, Converting the signal-recycling cavity into an unstable optomechanical filter to enhance the detection bandwidth of gravitational-wave detectors, *Phys. Rev. D* **99**, 102001 (2019).
[13] S. Daryanoosh, S. Slussarenko, D. W. Berry, H. M. Wiseman, and G. J. Pryde, Experimental optical phase measurement approaching the exact Heisenberg limit, *Nature*

- Communications **9**, 1 (2018).
- [14] D. V. Tsarev, S. M. Arakelian, Y. L. Chuang, R. K. Lee, and A. P. Alodjants, Quantum metrology beyond Heisenberg limit with entangled matter wave solitons, *arXiv* **26**, 19583 (2018).
 - [15] J. Huang, M. Zhuang, B. Lu, Y. Ke, and C. Lee, Achieving Heisenberg-limited metrology with spin cat states via interaction-based readout, *Phys. Rev. A* **98**, 1 (2018).
 - [16] S. Zhou, M. Zhang, J. Preskill, and L. Jiang, Achieving the Heisenberg limit in quantum metrology using quantum error correction, *Nature Communications* **9** (2018).
 - [17] V. Peano, H. G. L. Schwefel, C. Marquardt, and F. Marquardt, Intracavity Squeezing Can Enhance Quantum-Limited Optomechanical Position Detection through Deamplification, *Phys. Rev. Lett.* **115**, 243603 (2015).
 - [18] M. Korobko, L. Kleybolte, S. Ast, H. Miao, Y. Chen, and R. Schnabel, Beating the Standard Sensitivity-Bandwidth Limit of Cavity-Enhanced Interferometers with Internal Squeezed-Light Generation, *Phys. Rev. Lett.* **118** (2017).
 - [19] M. Korobko, Y. Ma, Y. Chen, and R. Schnabel, Quantum expander for gravitational-wave observatories, *Light: Science and Applications* **8**, 118 (2019).
 - [20] X. Li, M. Goryachev, Y. Ma, M. Tobar, C. Zhao, R. X. Adhikari, and Y. Chen, Broadband sensitivity improvement via coherent quantum feedback with PT-symmetry, *arXiv:2012.00836 [quant-ph]*, 81 (2021).
 - [21] X. Li, J. Smetana, A. Ubhi, J. Bentley, Y. Chen, Y. Ma, H. Miao, and D. Martynov, Enhancing interferometer sensitivity without sacrificing bandwidth and stability : beyond single-mode and resolved-sideband approximation, In preparation, 1 (2021).
 - [22] J. Bentley, H. Nurdin, Y. Chen, and H. Miao, Direct approach to realizing quantum filters for high-precision measurements, *Phys. Rev. A* **103**, 013707 (2021).
 - [23] V. B. Braginsky and F. Khalilli, *Quantum Measurement* (Cambridge University Press, 1992).
 - [24] N. Yamamoto, Coherent versus measurement feedback: Linear systems theory for quantum information, *Physical Review X* **4**, 10 (2014).
 - [25] M. Tsang and C. M. Caves, Evading quantum mechanics: Engineering a classical subsystem within a quantum environment, *Physical Review X* **2**, 1 (2012).
 - [26] H. I. Nurdin, M. R. James, and A. C. Doherty, Network Synthesis of Linear Dynamical Quantum Stochastic Systems, *SIAM J. Control. Optim.* **48**, 2686 (2009).
 - [27] H. I. Nurdin and N. Yamamoto, *Linear Dynamical Quantum Systems: Analysis, Synthesis, and Control* (Springer, 2017).
 - [28] C. M. Caves and B. L. Schumaker, New formalism for two-photon quantum optics. I. Quadrature phases and squeezed states, *Phys. Rev. A* **31**, 3068 (1985).
 - [29] B. L. Schumaker and C. M. Caves, New formalism for two-photon quantum optics. II. Mathematical foundation and compact notation, *Phys. Rev. A* **31**, 3093 (1985).
 - [30] H. Miao, H. Yang, and D. Martynov, Towards the design of gravitational-wave detectors for probing neutron-star physics, *Phys. Rev. D* **98**, 044044 (2018).
 - [31] M. R. James, H. I. Nurdin, and I. R. Petersen, H^∞ control of linear quantum stochastic systems, *IEEE T. Automat. Contr.* **53**, 1787 (2008).
 - [32] A. J. Shaiju and I. R. Petersen, A frequency domain condition for the physical realizability of linear quantum systems, *IEEE T. Automat. Contr.* **57**, 2033 (2012).
 - [33] J. Mizuno, Comparison of optical configurations for laser interferometric gravitational wave detectors, *Thesis* (1995).
 - [34] C. W. Gardiner and P. Zoller, *Quantum Noise: A Handbook of Markovian and Non-Markovian Quantum Stochastic Methods with Applications to Quantum Optics*, 2nd ed. (Springer, 2004).
 - [35] A. A. Clerk, M. H. Devoret, S. M. Girvin, F. Marquardt, and R. J. Schoelkopf, Introduction to quantum noise, measurement, and amplification, *Rev. Mod. Phys.* **82**, 1155 (2010).
 - [36] Y. Chen, Macroscopic quantum mechanics: Theory and experimental concepts of optomechanics, *J. Phys. B: At. Mol. Opt. Phys.* **46**, 104001 (2013).
 - [37] M. Aspelmeyer, T. J. Kippenberg, and F. Marquardt, Cavity optomechanics, *Rev. Mod. Phys.* **86**, 1391 (2014).
 - [38] C. M. Bender, Introduction to PT-symmetric quantum theory, *Contemporary Physics* **46**, 277 (2005).
 - [39] A. Buonanno and Y. Chen, Scaling law in signal recycled laser-interferometer gravitational-wave detectors, *Phys. Rev. D* **67** (2003).
 - [40] J. Gough and M. R. James, The series product and its application to quantum feedforward and feedback networks, *IEEE T. Automat. Contr.* **54**, 2530 (2009).